CHEMISTRY
A EUROPEAN JOURNAL

DOI: 10.1002/chem.200600767

Memory Effect of Activated Mg–Al Hydrotalcite: In Situ XRD Studies during Decomposition and Gas-Phase Reconstruction

Javier Pérez-Ramírez,*[a, b] Sònia Abelló,[a] and Niek M. van der Pers[c]

Abstract: The thermal decomposition of Mg–Al hydrotalcite and the subsequent reconstruction of the decomposed products in the presence of water vapor (2 vol. % H_2O in N_2) have been investigated by in situ XRD. Thermographic analysis and temperature-programmed desorption MS results complemented the diffraction data. Valuable mechanistic and kinetic insights into these processes, which are of prime importance for optimal activation of this type of material for catalytic applications, were obtained. Hydrotalcite decomposition to the mixed oxide proceeds via formation at 423–473 K of an intermediate phase, consisting of a highly disordered, dehydrated, layered structure. The latter evolves by removal of interlayer water on heating, causing a shrinking of the interlayer space (it is up to 45 % smaller than in the as-synthesized hydrotalcite). Above 623 K, $Mg(Al)O_x$ oxide with the periclase structure is formed. Reversion of the intermediate dehydrated structure to hydrotalcite upon contact with water vapor is complete and very fast at room temperature. Recovery of hydrotalcite from the oxide calcined at 723 K is two orders of magnitude slower than rehydration of the intermediate layered structure and one order of magnitude slower than the typically practiced liquid-phase reconstruction. In contrast to the decomposition, the reconstruction mechanism does not involve an intermediate phase. The gas-phase rehydration and reconstruction was interrupted above 303 K. This is attributed to the poor wetting of the surface of the decomposed materials induced by hampered H_2O adsorption above room temperature at the water vapor pressure applied. The Avrami–Erofe′ev model describes the reconstruction kinetics well.

Keywords: clays · decomposition · hydrotalcite · in situ XRD · kinetics · memory effect · reconstruction

Introduction

Layered double hydroxides or synthetic anionic clays with the hydrotalcite structure have received increasing attention in recent years due to their wide spectrum of applications as anion exchangers, adsorbents, ionic conductors, catalyst precursors, and catalyst supports.[1–3] As outlined by Allman[4] and Taylor,[5] these materials have the general formula $[M^{2+}_{1-x}M^{3+}_{x}(OH)_2][X^{m-}]_{xm}{}^{-1}\cdot nH_2O$ and can be visualized structurally as brucite-type octahedral layers, in which M^{3+} cations substitute partially for M^{2+} cations. The positive charge resulting from this substitution is balanced by anions (often carbonate) and water molecules arranged in interlayers alternating with the octahedral layers.

The ability to accommodate a large variety of di- and trivalent cations, and the formation of high-surface-area and well-dispersed mixed oxides upon thermal decomposition, are key aspects for the successful application of hydrotalcite-like compounds in catalysis.[6,7] Another unusual feature is the memory effect, by which the resulting oxide can recover the original hydrotalcite structure upon contact with water or aqueous solutions containing certain anions.[8,9] This property makes it possible to intercalate specific anions in the interlayer space, leading to applications as anion scavengers in water detoxification.[10,11] New functionalities have been also introduced by the intercalation of polyoxometalates and oxo, cyano, and halo complexes for the synthesis of pillared clays used as catalysts.[8] Recently, the memory effect has been applied for developing of a controlled-re-

[a] Prof. Dr. J. Pérez-Ramírez, Dr. S. Abelló
Laboratory for Heterogeneous Catalysis
Institute of Chemical Research of Catalonia (ICIQ)
Av. Països Catalans 16, 43007 Tarragona (Spain)
Fax: (+34) 977-920-224
E-mail: jperez@iciq.es

[b] Prof. Dr. J. Pérez-Ramírez
Catalan Institution for Research and Advanced Studies (ICREA)
Pg. Lluís Companys 23, 08010 Barcelona (Spain)

[c] Ing. N. M. van der Pers
Department of Materials Science and Engineering
Delft University of Technology
Faculty of 3 mE, Mekelweg 2, 2628 CD Delft (The Netherlands)

lease drug delivery system. To this end, amino acids and enzymes can be immobilized in hydrotalcites by thermal decomposition and reconstruction in the presence of the desired anionic species, inducing the later pharmacological action.[12]

Active solid-base catalysts with applications in numerous organic syntheses originate from the decomposition and subsequent retrotopotactic transformation of Mg–Al hydrotalcite. As shown schematically in Figure 1, the activation of the as-synthesized hydrotalcite is initiated by its thermal decomposition, leading to a high-surface-area $Mg(Al)O_x$ mixed oxide with strong O^{2-} Lewis basic sites. This material displays high activity in base-catalyzed reactions, including epoxidation,[13] dehydrogenation,[14] condensation,[15,16] Meerwein–Ponndorf–Verley reduction,[17] and transesterification.[18] Reconstruction of the oxide with water vapor or by immersion in decarbonated water (memory effect) leads to meixnerite,[1,6,19–21] a hydrotalcite analogue with OH^- groups as compensating anions in the interlayer instead of the original carbonates. The latter structure possesses Brønsted basic character and efficiently catalyze a number of organic reactions such as the self- and cross-aldol condensation of aldehydes and ketones,[19,21] Knoevenagel and Claisen–Schmidt condensation,[22,23] and Michael addition.[24]

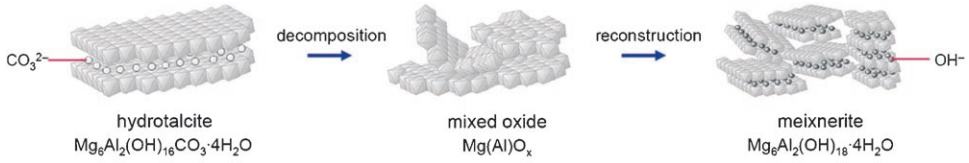

Figure 1. Activation of Mg–Al hydrotalcite by thermal decomposition followed by reconstruction. The mixed oxide and meixnerite materials exhibit a remarkable catalytic performance over a wide spectrum of important organic syntheses.

The catalytic properties of hydrotalcite-derived oxides and reconstructed materials depend largely on the sequence and specific conditions of the activation steps.[25–31] Consequently, monitoring the changes that occur in the structure during activation is crucial for the proper utilization of the resulting material in catalytic applications. In situ analysis of decomposition and reconstruction of layered double hydroxides is highly preferred rather than arresting the reaction and analyzing the product thereby obtained (ex situ approach). This is because the latter quenching process often affects the reaction product, and hence what is isolated is never guaranteed to be typical of the reaction matrix.[32,33] Structural changes during thermal decomposition of hydrotalcites have been assessed validly in situ by means of TGA-DTA-MS, HT-XRD, XAFS, and FT-IR and Raman spectroscopy.[25–31] Conversely, detailed studies during reconstruction of the resulting oxide back to the layered double hydroxide are scarce and typically have been analyzed ex situ. In these, samples have been characterized under ambient conditions after exposure to the reconstruction environment (for example, steam, decarbonated water, or aqueous solutions of NH_4OH or Na_2CO_3).

Exceptionally, Millange et al.[25] investigated the in situ reconstruction behavior of calcined Mg–Al hydrotalcite in aqueous sodium carbonate solution at 298–393 K by energy-dispersive X-ray diffraction (EDXRD) using white-beam synchrotron-generated X-rays. This well-founded fundamental study has limited relevance for the specific application of hydrotalcites in base catalysis, since reconstruction has to be practiced in the absence of carbonates and carbon dioxide in order to achieve the highest possible concentration of basic OH^- groups in the interlayer (see Figure 1). Van Bokhoven et al.[26] studied changes in the metal coordination of Mg–Al hydrotalcite upon calcination and rehydration in a water-saturated nitrogen flow by means of in situ XAFS at the Mg and Al K-edges. This work provided valuable mechanistic insights into the above transformations, but kinetic information was not derived.

Following these studies, we report a detailed in situ X-ray diffraction study to investigate quantitatively the mechanism and kinetics associated with the rehydration and reconstruction in the presence of steam of Mg–Al hydrotalcite decomposed at different temperatures. The observations from diffraction studies have been substantiated by application of TGA and TPD-MS (temperature-programmed desorption MS) techniques. The reconstruction process has been modeled in order to obtain relevant kinetic parameters. The outcome of our investigations is of importance for the optimal activation of hydrotalcite clays for catalytic applications.

Results and Discussion

Throughout this paper, the differently treated materials are denoted as HT-x, where the suffix x refers to the as-synthesized (as), dehydrated (dh), calcined (ca), rehydrated (rh), and reconstructed (rc) samples. Briefly, HT-dh and HT-ca are obtained by thermal treatment of HT-as at 473 and 723 K, respectively. HT-rh and HT-rc result from exposing HT-dh and HT-ca to steam, respectively (for details see the Experimental Section).

As-synthesized hydrotalcite: Chemical analysis of the as-synthesized Mg–Al hydrotalcite (HT-as) and thermogravimetry experiments revealed the chemical composition $Mg_{0.737}Al_{0.263}(OH)_2(CO_3)_{0.131}{\cdot}0.76\,H_2O$. This indicated that the Mg/Al molar ratio in the solid (2.8) was very close to the nominal value (3), confirming that the precipitation step was carried out effectively. The XRD cell (Figure 2) is described in the Experimental Section.

At 303 K (Figure 3) the hydrotalcite structure is the only crystalline phase (powder diffraction file 89-460 from the International Centre for Diffraction Data, ICDD). Assuming a 3R stacking of the layers and from the positions of the

Figure 2. In situ XRD cell used for thermal decomposition and reconstruction studies (left) and detail of the specimen mounting on the Pt_{90}–Rh_{10} alloy heater strip (right).

basal (003) reflection at $2\theta = 11.4°$ and nonbasal (110) reflection at $2\theta = 60.5°$, the lattice parameters were calculated as $c = 2.33$ nm and $a = 0.31$ nm. The average crystallite size of the sample was estimated using the Scherrer method[34] in both the (003) and the (110) reflections, taking the corresponding instrumental line broadening into account. This resulted in crystallites of 6.4 and 23 nm in the *c* and *a* directions, respectively. The longer dimension in the *a* direction can be expected from the well-known platelet-like morphology of hydrotalcite crystallites.[1] A representative transmission electron micrograph (Figure 4) of the as-synthesized sample shows platy particles, thickness 6–20 nm and lateral size 20–60 nm, in which a large number of crystallites are grouped together. The BET surface area and pore volume of HT-as derived from N_2 adsorption at 77 K were 69 $m^2 g^{-1}$ and 0.29 $cm^3 g^{-1}$, respectively.

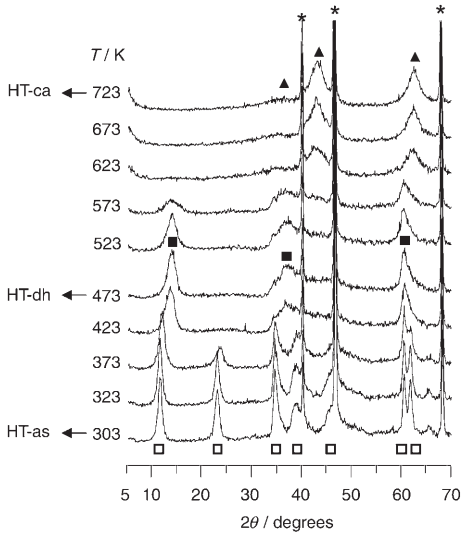

Figure 3. In situ XRD patterns during thermal decomposition of HT-as in N_2 at different temperatures: □: hydrotalcite, ■: dehydrated hydrotalcite, ▲: periclase, *: Pt_{90}–Rh_{10}.

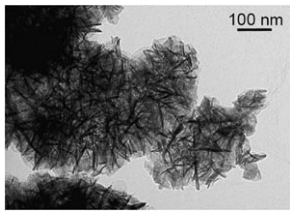

Figure 4. TEM of the as-synthesized Mg–Al hydrotalcite.

Thermal decomposition: Several studies have investigated the in situ thermal decomposition of hydrotalcite-like compounds. High-temperature X-ray diffraction provides valuable information on phase transitions of the sample.[27] This can be complemented with spectroscopic techniques for insights into changes upon heating of metal coordination (for example, XAFS, ^{27}Al MAS-NMR)[26,35] and of chemical species such as interlayer water, hydroxyls, and carbonate groups (for example, FT-IR, Raman, TGA-MS).[30,33] The in situ XRD patterns upon decomposition of HT-as in the range 303–723 K (Figure 3) are described and discussed with attention to a) the dehydration of the hydrotalcite at 303–473 K, b) the decomposition of the intermediate dehydrated phase at 473–573 K, and c) the formation of the mixed-oxide phase above 623 K.

Removal of interlayer water in the range 303–473 K is evidenced by the progressive shift of the (003) reflection at $2\theta = 11.4°$ to higher angles above 323 K, which can be interpreted as a decrease in basal spacing from 0.77 nm at 303 K to 0.64 nm at 473 K. In addition, the (003) reflection broadens upon heating, suggesting that the long-range ordering in the dehydrated sample is decreased in comparison with the as-synthesized hydrotalcite. The intensity of the characteristic (006), (009), and (113) reflections at $2\theta = 22$, 35, and 61.7°, respectively, decreased remarkably between 323 and 373 K, and had virtually disappeared at 423 K. At this temperature a very broad reflection centered at $2\theta = 36°$ appeared, coexisting with the basal (003) and nonbasal (110) reflections. The latter also broadened when the temperature was increased, becoming asymmetric, but its position was not affected with respect to the pattern at room temperature, revealing that the *a* parameter was not altered significantly upon dehydration. The XRD patterns at 423 and 473 K were very similar, and can be considered as characteristic for what we can define as dehydrated layered hydrotalcite (HT-dh). The occurrence of the three broad diffraction lines at $2\theta = 13.8$, 36, and 60.4° and particularly their simultaneous disappearance at 623 K (see Figure 3) was strong experimental evidence for assigning them to the same phase, with distinctive structural features compared with the original hydrotalcite.

Kanezaki was the first to report the formation of a metastable phase upon thermal treatment of Mg–Al hydrotalcite at 453 K.[27,28] He postulated that this phase results from the reaction of interlayer water with carbonates, leading to the formation of a hydroxyl-containing intermediate phase characterized by a *d* spacing of 0.66 nm. The latter is very similar to that determined in our HT-dh sample (0.64 nm). Unfortunately, the interaction of water and carbonates upon dehydration was merely speculative and not supported experimentally. Later studies using ^{27}Al MAS-NMR and HT-XRD,[25,30,35,36] and the present work have corroborated the occurrence of an intermediate phase around 423–473 K, where the layered structure is retained. However, the broad-

ening of the reflections characteristic of this phase in the patterns at 423 or 473 K in Figure 3 (particularly that emerging at $2\theta = 36°$), the disappearance of the (006) diffraction line and the associated decrease in the interlayer space imply an important disorder in the stacking of the layers. In opposition to Kanezaki's hypothesis,[27,28] many authors ruled out the water–carbonate interaction as the cause of HT-dh formation.[25,30,35,37] This argument has been supported by results from TGA, FT-IR, and MS, which have shown that CO_2 evolution upon carbonate decomposition occurs well above 523 K. The first weight loss step in the TGA upon thermal decomposition of HT-as (Figure 5) occurs below 500 K and amounts approximately 17%. This transition has been typically attributed to interlayer water removal,[35,38–40] which is corroborated by MS analysis of the gaseous products evolved. As clearly shown in Figure 5, H_2O was the only product of decomposition below 500 K, and formation of CO_2 was apparent only above 573 K. Based on these results, the involvement of carbonate groups in the dehydration step can be categorically excluded.

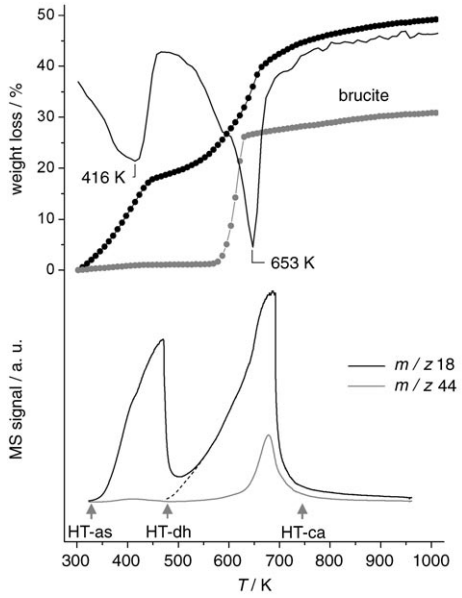

Figure 5. TGA-DTG curves of HT-as and the profiles of the H_2O and CO_2 products evolved during TPD-MS in N_2. Heating rate = 5 K min^{-1}.

Some reports have indicated that dehydroxylation of the brucite-like layers occurs simultaneously with the removal of interlayer water in the formation of the dehydrated phase.[30,37] Accordingly, it is also relevant to determine the degree of dehydroxylation in HT-dh. As shown by the signal at m/z 18 in Figure 5, the first and second stages of water formation overlap slightly around 500 K. The same is observed in the thermogravimetric profiles in Figure 5, where the first and second weight loss transitions are not separated clearly in temperature by a well-defined plateau. Based on this, some dehydroxylation of the brucite-like layers in the relevant temperature range where HT-dh is formed cannot be excluded. In situ XAFS and ^{27}Al MAS-NMR studies have proven that the dehydroxylation of Mg–Al hydrotalcite starts at 473 K, as indicated by the change in coordination of the Mg and Al centers.[26,35,36] This temperature coincides with that obtained by extrapolating the tail of the second H_2O peak from the MS analysis to the baseline (broken line in Figure 5). Consequently, the dehydroxylation occurs to only a minor degree at the temperature where the intermediate dehydrated structure is formed. This can be reinforced further from the TGA profile of a reference brucite sample, $Mg(OH)_2$. The weight loss in this sample is due only to dehydroxylation, since neither interlayer water nor carbonate groups are contained in the structure. The gray profile in Figure 5 shows that no significant weight loss occurs upon heating to 573 K. Based on this, we infer that the changes in the hydrotalcite structure occurring below 473 K are solely a consequence of the removal of water from the interlayer space.

The dehydration of the layered double hydroxide can be quantified by determination of the interlayer space from the basal reflection at $2\theta = 11$–$13°$. The interlayer space in HT-as is defined as the distance between two hydroxyl groups in adjacent layers (Figure 6), and can be calculated as the difference between the basal c spacing from the XRD pattern (0.77 nm) and the thickness of the brucite sheet (0.48 nm).[1] In this manner, the layer-to-layer distance in HT-as amounts to 0.29 nm (Figure 6), which is in excellent agreement with the 0.3 nm value reported by Allmann from X-ray crystallographic data.[4] The structural scheme in the figure takes into account that the symmetry axes of both water (C_2) and carbonate (C_3) species are perpendicular to the layers, as demonstrated by ^{1}H and ^{13}C NMR studies.[41]

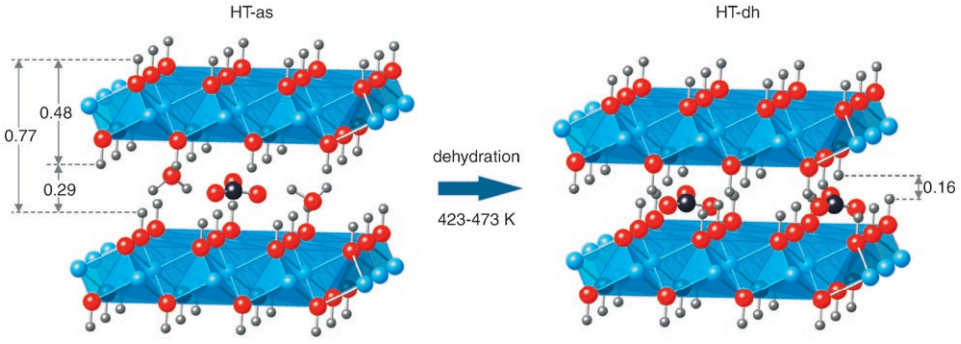

Figure 6. Schematic representation of HT-as and HT-dh. Dimensions are given in nm.

As shown in Figure 7, the interlayer space decreased abruptly in the range 350–450 K down to approximately

0.16 nm, which is equivalent to shrinkage of the interlayer space in HT-dh by around 45% with respect to HT-as (see Figure 6). This value is very close to the thickness of the carbonate anion if located with its C_3 axis perpendicular to the brucite-like sheets (0.14 nm).[41] In situ FT-IR investigations have demonstrated that dehydration of the interlayer space in hydrotalcites causes the reorganization of the carbonate anions in the interlayer, evidenced by the splitting of the ν_3 mode at 1370 cm^{-1} into two absorption bands around 1520 and 1360 cm^{-1}.[26,39,42] The latter is due to the loss of symmetry from D_{3h} in as-synthesized hydrotalcites to C_s, C_{3v}, or C_{2v} symmetry in dehydrated hydrotalcites.[43,44] The lower degree of symmetry of CO_3^{2-} ions in HT-dh can be envisaged intuitively from the restricted degree of freedom of these species in the confined interlayer space and the likely increase in electronic repulsion of carbonate groups in the absence of water.

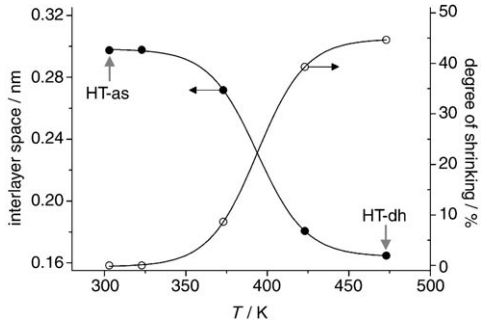

Figure 7. Variation of the interlayer space with temperature during dehydration of HT-as, and the resulting degree of shrinking.

Figure 3 shows that the formation of the mixed oxide $Mg(Al)O_x$ occurs at 623 K, to the detriment of the dehydrated layered phase. Reflections at $2\theta = 37$, 43, and 62° are characteristic of the rock-salt periclase structure (MgO, powder diffraction file 45-0946 from ICDD). The collapse of the intermediate layered structure into the oxide phase is a consequence of the dehydroxylation of the brucite-like sheets by condensation of neighboring OH groups in the layers. This process occurs in the broad range 473–723 K according to TGA and TPD-MS (Figure 5). The occurrence of a single weight loss in the range 500–723 K, and the fact that the maximum of the H_2O and CO_2 profiles in MS analysis coincide, are evidence of the coupling between dehydroxylation and decarbonation processes.[26,30] However, while formation of water has already started at 500 K, CO_2 is evolved only above 573 K. It can thus be concluded from this result that dehydroxylation precedes carbonate decomposition.

Rehydration of the intermediate layered structure: The transformation of the intermediate dehydrated phase back to hydrotalcite was investigated by in situ XRD. The sample treated at 473 K (HT-dh) was cooled in dry N_2 to a temperature in the range 303–423 K and then contacted with moisturized N_2 (2 vol.% H_2O). Figure 8 shows the XRD patterns upon rehydration at two representative temperatures and different times from the moment at which the inlet N_2 flow was saturated with water ($t = 0$ min). The reference pattern of the as-synthesized hydrotalcite HT-as is also shown. In the first rehydration test at 303 K, the 2θ range scanned was the same as in the thermal decomposition studies (5–70°), but it had to be narrowed to 5–25° in order to follow the rehydration process properly. In this range, the representative basal diffraction line can be monitored. Recovery of the hydrotalcite upon exposure of HT-dh to steam was very fast at 303 K, as can be concluded qualitatively from the marked shift of the basal reflection from $2\theta = 13.8$ to 11° in the first 5 min in the H_2O-containing flow.

The degree of rehydration is quantified in Figure 9, following the evolution of the interlayer space (determined as described in the previous section). The characteristic 0.16 nm space in HT-dh increases steeply due to accommodation of water molecules in the interlayer space, reaching the original value in HT-as (0.29 nm) after a brief period of 6 min. This is in excellent agreement with XAFS results published by van Bokhoven et al.,[26] showing that the changes in coordination of Mg and Al upon treatment of

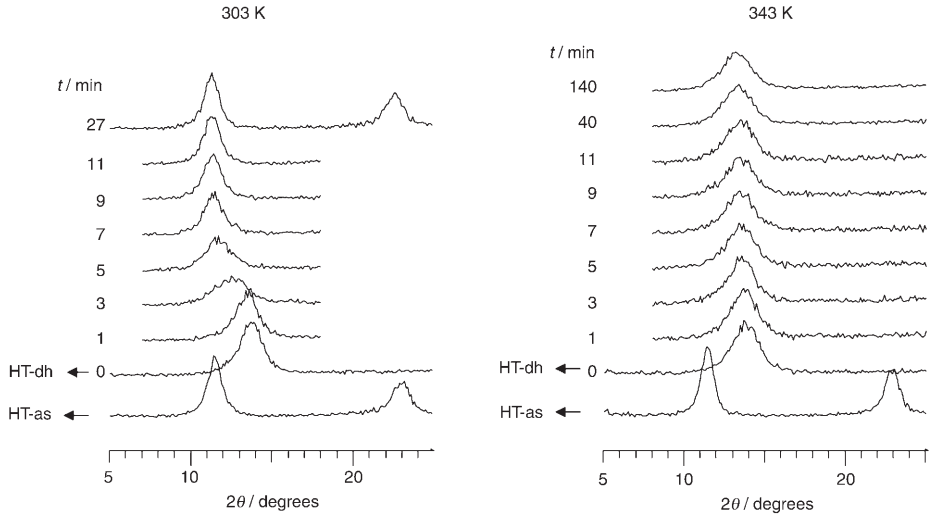

Figure 8. In situ XRD patterns during rehydration of HT-dh at 303 and 343 K in a N_2 flow with 2 vol% H_2O.

the hydrotalcite in the range 425–475 K are fully reversible after cooling the sample to room temperature.

Kanezaki[27] also observed the recovery of the original hydrotalcite upon contact of the metastable dehydrated phase

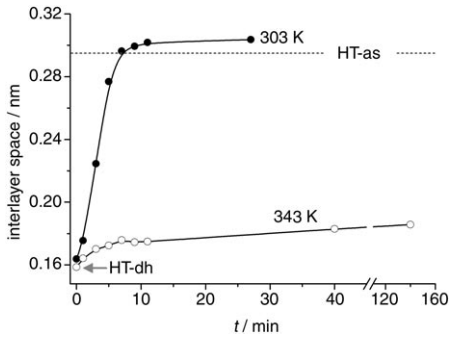

Figure 9. Variation of interlayer space with time upon rehydration of HT-dh at 303 and 343 K in a N_2 flow with 2 vol% H_2O.

with a humid atmosphere at room temperature. In our case, an even faster rehydration of HT-dh at 303 K could have been monitored if a smaller cell had been used in the XRD experiments. About 10 min are required from saturation of the N_2 flow by water until the gas concentration in the chamber reaches the target value of approximately 2 vol% (Figure 10), due to its relatively large volume ($\approx$1 L).

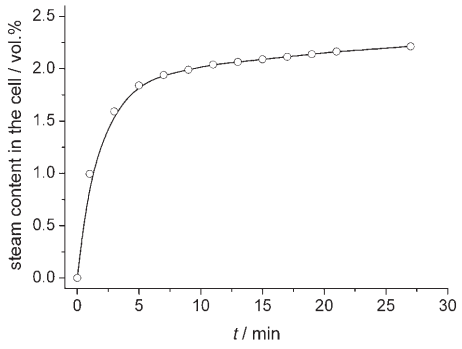

Figure 10. Characteristic curve of the increase in steam content in the XRD cell with time upon saturation of the N_2 flow with water.

Two additional observations related to the rehydration mechanism can be extracted from our in situ XRD measurements. First, Figure 8 shows that the transition during rehydration at 303 K between 1 and 3 min causes not only a shift in the position of the basal reflection, but also a substantial broadening and decreased intensity. The gradual shifting continues in the pattern at 5 min, but contrarily to that at 3 min, the (003) reflection begins to sharpen again. This reveals that rehydration involves not only the physical filling of the interlayer space by water molecules, but also a phase transition from the disordered, dehydrated, layered phase back to the original hydrotalcite. Figure 9 also demonstrates that rehydration times longer than 7 min lead to a greater interlayer space than in the original hydrotalcite (increased by approximately 10%), which is not further changed with time up to 30 min. This could suggest that the interlayer of the rehydrated product can accommodate more water than the as-synthesized hydrotalcite. Several authors have reported the re-expansion of the original spacing if the hydrotalcite is not heated above 573 K.[1] However, the relative error in the determination of the interlayer space can be estimated as 3–5%, so no definitive conclusions on this effect can be drawn.

For the first time, it has been observed that the HT-dh phase can be stabilized when the sample is slightly above room temperature. The basal reflection of HT-dh at $2\theta = 13.8°$ hardly changed after 2 h of exposure to a wet atmosphere at 343 K (Figure 8). As a consequence, the increase in the interlayer space during this period was only about 15% (Figure 9). As expected, no rehydration was evidenced upon further increasing the temperature to 423 K. This aspect is discussed further in the next section.

Reconstruction of the mixed oxide: The reconstruction of the calcined Mg–Al hydrotalcite at 723 K (HT-ca) was investigated by following the same experimental protocol as described for the rehydration of HT-dh. Figure 11 shows the evolution of the diffraction patterns with time upon bringing HT-ca into contact with the moisturized nitrogen flow at two selected temperatures. The mixed oxide $Mg(Al)O_x$ recovers the hydrotalcite structure gradually at 303 K. The characteristic diffraction lines of hydrotalcite start to appear slightly after 3 h in contact with steam. At longer times, the reflections of the hydrotalcite phase progressively intensify and sharpen, particularly in the 3–12 h period. These changes are coupled to the decreased reflections of the periclase phase. After 21 h, the fact that the main reflection of the oxide phase at $2\theta = 43°$ cannot be discerned could indicate qualitatively that the reconstruction of the original hydrotalcite-like structure has been virtually completed. At this time, it is also possible to distinguish the characteristic (110) and (113) reflections of the hydrotalcite structure at diffraction angles around $2\theta = 60.4$ and 61.7°. By this reconstruction process the hydrotalcite analogue meixnerite is obtained, as hydroxyls act as compensating anions in the interlayer instead of carbonates (see Figure 1). This process differs from HT-dh rehydration, since only water is lost upon heating at 473 K (see section on thermal decomposition above).

The patterns in Figure 11 at 303 K indicate that reconstruction of HT-ca does not go through the layered dehydrated phase described earlier, since the (003) reflection shifted to $2\theta = 13.8°$ and the very broad reflection at $2\theta = 36°$ was not observed at an intermediate stage. In fact, the interlayer space was almost identical to that in HT-as during the whole reconstruction process. This observation indicates that the retrotopotactic transformation occurs in a single step (mixed oxide→meixnerite), in contrast with the two-stage transition during decomposition (hydrotalcite→dehydrated layered phase→mixed oxide). In view of this, hydroxylation of the oxide structure and filling of the interlayer space by water are simultaneous, contrarily to the sequence in thermal decomposition.

The evolution of the degree of reconstruction (α) of HT-ca with time was determined experimentally at 303 K by comparing the area under the (003) diffraction line in each

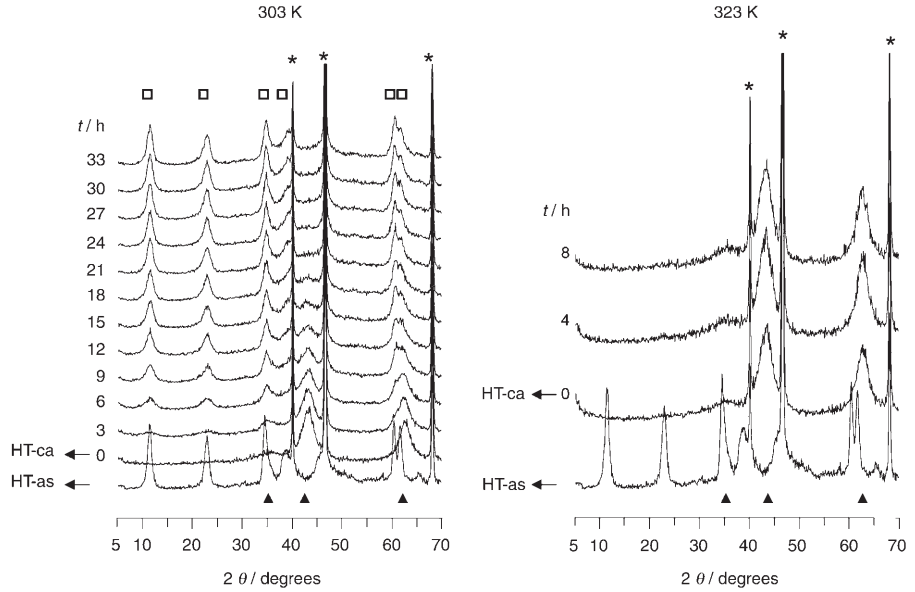

Figure 11. In situ XRD patterns during reconstruction of HT-ca at 303 and 343 K in a N_2 flow with 2 vol % H_2O. □: Hydrotalcite, ▲: periclase, *: Pt_{90}–Rh_{10}.

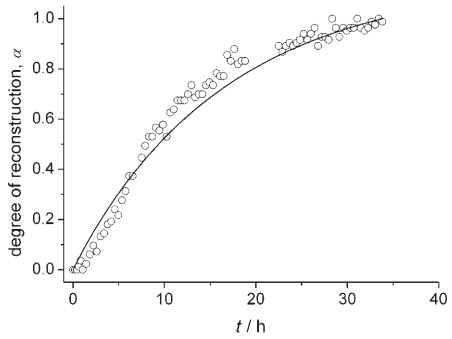

Figure 12. Experimental (○) and calculated degree of reconstruction (——) of HT-ca versus exposure time at 303 K in a N_2 flow with 2 vol % H_2O.

pattern with the area of the (003) diffraction line in the pattern at 33 h (assumed to be a totally reconstructed sample). The values obtained (open circles in Figure 12) show a quasi-linear reconstruction up to 20 h, approaching a plateau at longer times. Comparing the time scales in Figure 8 and Figure 11, the gas-phase reconstruction of HT-ca is concluded to be two orders of magnitude slower than the rehydration of HT-dh. As shown in Figure 11, the reconstruction of HT-ca at temperatures slightly above ambient (at 323 K, for example) failed to occur after an 8 h exposure to the wet atmosphere. A difference of only about 20 K above room temperature was sufficient to prevent reconstruction of the oxide. Reproducible results were obtained from the latter experiments repeated several times. The dramatic deceleration of the gas-phase reconstruction with temperature can be related to the limited wetting of the surface of the decomposed materials by impeded water adsorption on the solid material above room temperature. This is a required first step to initiate the rehydration reaction. In reconstruction studies reported in the literature, the calcined hydrotalcites have typically been immersed in aqueous solutions of Na_2CO_3[25,45,46] or NH_4OH.[47] In the latter case it took relatively short periods to fully recover the original hydrotalcite structure in aqueous solutions as compared to the gas-phase reconstruction practiced here. For example, Millange et al.[25] determined by means of EDXRD that a period of 3 h was sufficient to complete the reconstruction at room temperature of calcined Mg–Al hydrotalcite (at 673 K) in 0.8 M Na_2CO_3 aqueous solution. This process was accelerated by increasing the temperature, since dissolution of the poorly crystalline oxide in solid carbonate and nucleation of the reactive species so formed became faster. The faster reconstruction can be explained by the contact of liquid water with the oxide surface being much more favorable than in our gas-phase rehydration mode, due to the efficient wetting of the surface by the fluid. However, comparison of our work with reported studies in the liquid phase is not straightforward; the liquid-phase experiments have been performed in aqueous solutions with anions (for example, carbonates, hydroxides), which can be a factor influencing the kinetics of the reconstruction process. To the best of our knowledge, mechanistic studies in pure decarbonated water have not been reported. The *frozen* recovery of the original structure when elevating the sample temperature can be of practical relevance, since it seems to enable stabilization of intermediate (partially decomposed) structures during decomposition of anionic clays, even in wet environments.

To extract kinetic information, the reconstruction data at 303 K were fitted using the simple nucleation growth model proposed by Avrami and Erofe′ev[48] [Eq. (1)], where α is the degree of reconstruction, k is the rate coefficient, t is the time, and n is the Avrami exponent. This empirical equation has been applied widely to model crystallization and phase transformations in solid-state chemistry.[49,50]

$$\alpha = 1-\exp[-(kt)^n] \quad (1)$$

$$\ln[-\ln(1-\alpha)] = n\ln t + n\ln k \quad (2)$$

A good description of the experimental results was achieved (line in Figure 12). Sharp and Hancock[51] proposed the linearization of Equation (1) by taking the double logarithm, leading to Equation (2). This representation (Figure 13) enables determination of the rate coefficient $k = 2.26(\pm 0.06) \times 10^{-5}\ s^{-1}$ and the Avrami exponent $n = 1.39(\pm 0.03)$ at 303 K.

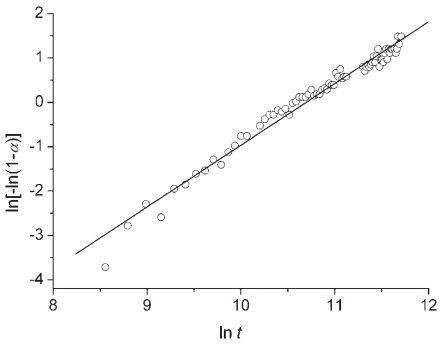

Figure 13. Sharp–Hancock plot for the reconstruction of HT-ca at 303 K.

The same approach was used previously by Millange et al.[25] to model the reconstruction of calcined Mg–Al hydrotalcite in aqueous solutions of Na_2CO_3, obtaining a rate coefficient approximately 10 times higher than in the gas-phase reconstruction with water vapor.

Conclusion

The development of instrumentation and appropriate procedures made it possible to gain insights into the mechanism and kinetics of the thermal decomposition of hydrotalcites and their subsequent gas-phase rehydration and reconstruction processes (memory effect). In situ XRD is a powerful technique to accomplish this, since it provides direct evidence on the nature of the phases present in the reaction and their relative concentration. This information is of great value for optimization of the activation of hydrotalcites for their utilization in catalytic applications. Hydrotalcite decomposition to the mixed oxide goes through an intermediate highly disordered layered phase, which is exclusively the product of interlayer water removal, causing a dramatic shrinkage of the space between brucite-like layers. The collapse of the layered structure is initiated above 523 K by condensation of hydroxyls from adjacent layers followed by carbonate decomposition, leading to a poorly crystalline $Mg(Al)O_x$ oxide. Recovery of hydrotalcite from the oxide calcined at 723 K is two orders of magnitude slower than rehydration of the intermediate layered structure and one order of magnitude slower than the liquid-phase reconstruction as typically practiced. In contrast to the decomposition, the reconstruction mechanism is direct; that is, it does not involve the occurrence of an intermediate phase. Above 303 K, the gas-phase reconstruction is hampered. This is attributed to the limited adsorption of water on the solid above room temperature, which causes poor wetting of the surface. This enables stabilization of partially decomposed phases by application of moderate temperatures. The Avrami–Erofe′ev model describes well the gas-phase reconstruction kinetics.

Experimental Section

Preparation of materials: Mg–Al hydrotalcite with a nominal Mg/Al molar ratio of 3:1 was prepared by coprecipitation at constant pH by the in-line dispersion–precipitation (ILDP) method.[52] Briefly, aqueous solutions $Mg(NO_3)_2{\cdot}6H_2O$ (0.75 M) and $Al(NO_3)_3{\cdot}9H_2O$ (0.25 M) and the precipitating agent (NaOH + Na_2CO_3, each 1 M) were fed continuously at room temperature by means of peristaltic pumps into a home-made micro-reactor (effective volume $\approx$6 cm^3). The pH was kept at 10 by using an in-line probe that measured the pH of the slurry directly at the outlet of the micro-reactor and was connected to one of the pumps for pH control. The precipitation chamber was stirred at 13 500 rpm by a high-speed disperser and the average residence time was fixed at 36 s. The resulting slurry was aged in a vessel under stirring (500 rpm) at 298 K for 12 h. The material was filtered, washed extensively with deionized water to remove Na^+ and NO_3^- ions, and dried at 353 K for 12 h. Brucite ($Mg(OH)_2$) was prepared as a reference sample by precipitation of Mg^{2+} ions following the same procedure, but using NaOH as the precipitating agent.

Characterization: The chemical composition of the as-synthesized Mg–Al hydrotalcite was determined by AAS (Hitachi Z-8200) and ICP-OES (Perkin–Elmer Plasma 400). The sample was dissolved in HNO_3 (10 wt %) before analysis. N_2 adsorption at 77 K was performed in a Quantachrome Autosorb 1-MP gas adsorption analyzer. Before analysis, the sample was evacuated at 393 K for 16 h. The BET method[53] was applied in the relative pressure range of 0.01–0.3 to calculate the total surface area. A Zeiss 10 CA microscope was used for TEM. Thermogravimetric analysis was carried out in a Mettler Toledo TGA/SDTA851e microbalance equipped with a 34-position sample robot. Analyses were performed on each sample ($\approx$3 mg) placed in a α-Al_2O_3 crucible (70 μL), in a dry N_2 flow (50 cm^3(STP) min^{-1}. The temperature was increased from 323 to 973 K at 5 K min^{-1}. To study the evolution of the gases during the decomposition of Mg–Al hydrotalcite by TPD-MS, the as-synthesized material ($\approx$100 mg) was decomposed in dry N_2 (50 cm^3(STP) min^{-1}) in a quartz fixed-bed reactor (10 mm i.d.). The temperature was raised from room temperature to 973 K at 5 K min^{-1} and masses m/z 18 (H_2O) and m/z 44 (CO_2) were monitored with a quadrupole mass spectrometer (Pfeiffer OmniStar GSD 301O).

In situ XRD: X-ray diffraction experiments were performed at ambient pressure in a Bruker-AXS D5005 θ–θ diffractometer equipped with a Bruker-AXS MRI high-temperature chamber (vol. $\approx$1 L)(Figure 2, left) and a diffracted beam graphite monochromator using $Cu_{K\alpha}$ radiation. A thin layer of sample ($\approx$30 mg) was mounted on the Pt_{90}–Rh_{10} heater strip inside the chamber (Figure 2, right) by placing a few droplets of a suspension of finely ground sample in ethanol on the strip, then drying under ambient conditions. Great care was taken to minimize the specimen displacement effect by checking the exact position of the heater strip before every experiment and carefully reproducing the specimen installation. Diffractograms were acquired for the Bragg–Brentano geometry in the range of $5 < 2\theta < 70°$ with a step size of 0.1° and a counting time per step in the range 1–6 s. Different experiments were carried out to investigate the thermal decomposition of the Mg–Al hydrotalcite as well as the rehydration and reconstruction of decomposed products at different temperatures:

- In situ XRD patterns during thermal decomposition in a N_2 flow (100 cm^3(STP) min^{-1}) were recorded at intervals of 50 K in the temperature range 303–723 K after equilibration of 10 min at each temperature. The heating rate was 5 K min^{-1}. The sample was directly heated by the noble metal alloy strip, whose temperature was controlled within $\pm$2 K. In the cell, the gas flow was positioned across the sample, thus ensuring good solid–gas contact.
- In situ rehydration was performed over the Mg–Al hydrotalcite previously treated in a dry N_2 flow at 473 K for 10 min to dehydrate the sample. This was followed by cooling in N_2 to a selected temperature in the range 303–423 K. Subsequently, the N_2 gas was moisturized with water by means of an Ansyco SYCOS-H humidity generator

and introduced to the chamber at a total flow rate of 100 cm^3 (STP) min^{-1}. XRD patterns were recorded continuously with time.

- In situ reconstruction experiments were carried out similarly to rehydration experiments, but the as-synthesized hydrotalcite was decomposed in a dry N_2 flow at 723 K for 5 h.

The temperature and relative humidity inside the chamber in the vicinity of the sample were monitored by a Novasina HygroDat 100 sensor. Under the conditions applied in the humidity generator, the steam content in the N_2 carrier for the rehydration and reconstruction experiments was $\approx$2 vol.% H_2O (RH 90%).

Acknowledgements

This work was supported financially by the ICIQ Foundation. G. Stoica is acknowledged for the synthesis of brucite and Dr. C. de Graaf for help with the structures in Figure 6.

[1] F. Cavani, F. Trifirò, A. Vaccari, *Catal. Today* **1991**, *11*, 173–301.
[2] P. S. Braterman, Z. P. Xu, F. Yarberry, in *Handbook of Layered Materials* (Eds.: S. M. Auerbach, K. A. Carrado, P. K. Dutta), Taylor & Francis, New York, **2004**, pp. 313–372.
[3] D. G. Evans, X. Duan, *Chem. Commun.* **2006**, 485–496.
[4] R. Allmann, *Acta Crystallogr. Sect. B* **1968**, *24*, 972–977.
[5] H. W. F. Taylor, *Mineral. Mag.* **1973**, *39*, 377.
[6] D. Tichit, B. Coq, *CATTECH* **2003**, *7*, 206–217.
[7] W. T. Reichle, *J. Catal.* **1985**, *94*, 547–557.
[8] V. Rives, M. A. Ulibarri, *Coord. Chem. Rev.* **1999**, *181*, 61–120.
[9] A. Vaccari, *Appl. Clay Sci.* **1999**, *14*, 161–198.
[10] L. P. Cardoso, J. B. Valim, *J. Phys. Chem. Solids* **2004**, *65*, 481–485.
[11] M. A. Ulibarri, I. Pavlovic, C. Barriga, M. C. Hermosin, J. Cornejo, *Appl. Clay Sci.* **2001**, *18*, 17–27.
[12] H. Nakayama, N. Wada, M. Tsuhako, *Int. J. Pharm.* **2004**, *269*, 469–478.
[13] S. Ueno, K. Yamaguchi, K. Yoshida, K. Ebitani, K. Kaneda, *Chem. Commun.* **1998**, 295–296.
[14] A. Corma, V. Fornés, F. Rey, *J. Catal.* **1994**, *148*, 205–212.
[15] J. I. Di Cosimo, C. R. Apesteguía, M. J. L. Ginés, E. Iglesia, *J. Catal.* **2000**, *190*, 261–275.
[16] Y. Ono, *J. Catal.* **2003**, *216*, 406–415.
[17] P. Kumbhar, J. Sanchez Valente, J. Lopez, F. Figueras, *Chem. Commun.* **1998**, 535–536.
[18] B. M. Choudary, M. L. Kantam, C. V. Reddy, S. Aranganathan, P. L. Santhi, F. Figueras, *J. Mol. Catal. A* **2000**, *159*, 411–416.
[19] K. K. Rao, M. Gravelle, J. Sanchez Valente, F. Figueras, *J. Catal.* **1998**, *173*, 115–121.
[20] J. C. A. A. Roelofs, A. J. van Dillen, K. P. de Jong, *Catal. Lett.* **2001**, *74*, 91–94.
[21] S. Abelló, F. Medina, D. Tichit, J. Pérez-Ramírez, J. C. Groen, J. E. Sueiras, P. Salagre, Y. Cesteros, *Chem. Eur. J.* **2005**, *11*, 728–739.
[22] M. J. Climent, A. Corma, S. Iborra, J. Primo, *J. Catal.* **1995**, *151*, 60–66.
[23] M. L. Kantam, B. M. Choudary, C. V. Reddy, K. K. Rao, F. Figueras, *Chem. Commun.* **1998**, *9*, 1033–1034.
[24] B. M. Choudary, M. L. Kantam, C. R. V. Reddy, K. K. Rao, F. Figueras, *J. Mol. Catal. A* **1999**, *146*, 279–284.
[25] F. Millange, R. I. Walton, D. O'Hare, *J. Mater. Chem.* **2000**, *10*, 1713–1720.
[26] J. A. van Bokhoven, J. C. A. A. Roelofs, K. P. de Jong, D. C. Koningsberger, *Chem. Eur. J.* **2001**, *7*, 1258–1265.
[27] E. Kanezaki, *Inorg. Chem.* **1998**, *37*, 2588–2590.
[28] E. Kanezaki, *Solid State Ionics* **1998**, *106*, 279–284.
[29] J. Pérez-Ramírez, G. Mul, J. A. Moulijn, *Vib. Spectrosc.* **2001**, *27*, 75–88.
[30] W. Yang, Y. Kim, P. K. T. Liu, M. Sahimi, T. Tsotsis, *Chem. Eng. Sci.* **2002**, *57*, 2945–2953.
[31] J. T. Kloprogge, R. L. Frost, *Appl. Catal. A* **1999**, *184*, 61–71.
[32] G. R. Williams, A. I. Khan, D. O'Hare, in *Structure and Bonding, Vol. 119* (Eds.: X. Duan, D. G. Evans), Springer, Berlin, **2006**, pp. 161–192.
[33] J. Pérez-Ramírez, G. Mul, F. Kapteijn, J. A. Moulijn, *J. Mater. Chem.* **2001**, *11*, 821–830.
[34] P. Scherrer, *Nachr. Ges. Wiss. Göttingen* **1918**, *2*, 98–103.
[35] J. Rocha, M. del Arco, V. Rives, M. A. Ulibarri, *J. Mater. Chem.* **1999**, *9*, 2499–2503.
[36] M. Bellotto, B. Rebours, O. Clause, J. Lynch, *J. Phys. Chem.* **1996**, *100*, 8535–8542.
[37] V. Rives, *Inorg. Chem.* **1998**, *38*, 406–407.
[38] D. Tichit, M. Naciri Bennani, F. Figueras, J. R. Ruiz, *Langmuir* **1998**, *14*, 2086–2091.
[39] J. I. Di Cosimo, V. K. Díez, M. Xu, E. Iglesia, C. R. Apesteguía, *J. Catal.* **1998**, *178*, 499–510.
[40] J. Pérez-Ramírez, S. Abelló, *Thermochim. Acta* **2006**, *444*, 75–82.
[41] A. van der Pol, B. L. Mojet, E. van de Ven, E. de Boer, *J. Phys. Chem.* **1994**, *98*, 4050–4054.
[42] F. Prinetto, G. Ghiotti, R. Durand, D. Tichit, *J. Phys. Chem. B* **2000**, *104*, 11117–11126.
[43] J. Pérez-Ramírez, G. Mul, F. Kapteijn, J. A. Moulijn, *Mater. Res. Bull.* **2001**, *36*, 1767–1775.
[44] V. Rives, *Mater. Chem. Phys.* **2002**, *75*, 19–25.
[45] T. Hibino, A. Tsunashima, *Chem. Mater.* **1998**, *10*, 4055–4061.
[46] M. Rajamathi, G. D. Nataraja, S. Ananthamurthy, P. V. Kamath, *J. Mater. Chem.* **2000**, *10*, 2754–2757.
[47] F. Prinetto, D. Tichit, R. Teissier, B. Coq, *Catal. Today* **2000**, *55*, 103–116.
[48] M. Avrami, *J. Chem. Phys.* **1939**, *7*, 1103–1112.
[49] A. M. Fogg, S. J. Price, R. J. Francis, S. O'Brien, D. O'Hare, *J. Mater. Chem.* **2000**, *10*, 2355–2357.
[50] A. J. Norquist, D. O'Hare, *J. Am. Chem. Soc.* **2004**, *126*, 6673–6679.
[51] J. H. Hancock, J. D. Sharp, *J. Am. Ceram. Soc.* **1972**, *55*, 74–77.
[52] S. Abelló, J. Pérez-Ramírez, *Adv. Mater.* **2006**, *18*, 2436–2439.
[53] S. Brunauer, P. H. Hemmet, E. Teller, *J. Am. Chem. Soc.* **1938**, *60*, 309–319.

Received: June 1, 2006
Published online: October 9, 2006

